contributions to the right-hand side of Eq. (18) and vertex terms all have leading terms of order α in the energy.

[32]G. Höhler, Nuovo Cimento 11, 691 (1955).
[33]G. R. Allcock, Advan. Phys. 5, 412 (1956).
[34]G. Höhler and Mullensiefen, Z. Physik 157, 159 (1959).
[35]Note that this is also the result obtained by Gross (see Ref. 16).
[36]T. D. Lee and D. Pines, Phys. Rev. 88, 960 (1952).
[37]D. Matz and B. C. Burkey, Solid State Commun. 8, 1887 (1970).

Raman Spectra of the Alkali Azides: KN_3, RbN_3, CsN_3 [†]

C. E. Hathaway and Paul A. Temple

Department of Physics, Kansas State University, Manhattan, Kansas 66502

(Received 23 October 1970)

The first-order Raman spectra of KN_3, RbN_3, and CsN_3, all of which possess a body-centered tetragonal crystal structure with the symmetry of the space group D_{4h}^{18}-$I4/mcm$, have been measured at room and liquid-nitrogen temperatures. The five Raman-active phonons predicted by group theory have been observed and assigned on the basis of the scattering tensors.

INTRODUCTION

Many of the solid inorganic azides decompose to give the simple products of the anion and nitrogen. This decomposition may be caused by heat, shock, light, or ionizing radiation. In the case of the heavy-metal azides the reaction can be highly exothermic. However, some of the azides, in particular the alkali azides, are more stable. Therefore the alkali azides have been the subject of many studies.

Considerable work has been done on the vibrational spectra of the alkali-metal azides. Bryant[1-4] has presented extensive infrared data on single crystals of sodium, potassium, and cesium azide and some mercury-arc Raman data on polycrystalline alkali azides. Recently, the long-wavelength translatory optical frequencies for KN_3, RbN_3, and CsN_3 have been measured by far-infrared transmission on polycrystalline samples.[5] Also an attempt has been made recently to calculate on the basis of a rigid-ion approximation the lattice vibrational frequencies of potassium, rubidium, and cesium azide.[6] Because of our interest in Raman scattering from radiation-induced defects in the alkali azides,[7,8] we have undertaken a study of the laser Raman spectra of these alkali azides. The present study has allowed a definitive assignment of the first-order Raman-active phonons.

Potassium, rubidium, and cesium azide possess a body-centered tetragonal crystal structure with the symmetry of the space group D_{4h}^{18}-$I4/mcm$.[9] The crystal structure is shown in Fig. 1. There are four formula units per crystallographic unit cell and two formula units per primitive cell. The crystallographic unit-cell parameters for these alkali azides are listed in Table I. As the effective ionic radius of the metal ion is increased the unit-cell dimensions are correspondingly increased. However, these changes are such that the contact radius between the metal ion and the end nitrogen of the azide ion is the same for all three materials.

Group theory indicates that the 24 deg of freedom for the 8 atoms in each primitive cell are divided into vibrations at $k = 0$ of the symmetries indicated
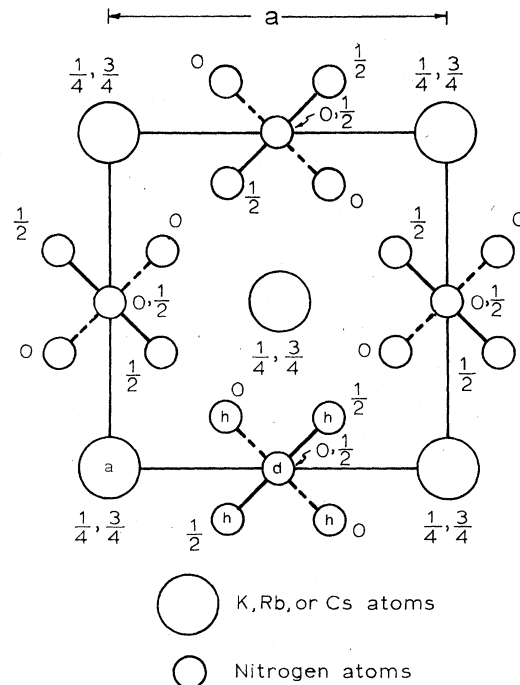
FIG. 1. Crystallographic unit cell of the alkali azides possessing the symmetry of the space group D_{4h}^{18}-$I4/mcm$. Letters a, d, and h refer to the special positions of D_{4h}^{18}. Fourfold z axis is normal to the figure.

TABLE I. Unit cell for K, Rb, and CsN$_3$.[a] Body-centered tetragonal, D_{4h}^{18}-$I4/mcm$ symmetry.

Cation	Cation radius (Å)	Cell constants a_0	(Å) c_0	Contact radius (Å)
K	1.33	6.094	7.056	1.63
Rb	1.48	6.36	7.41	1.63
Cs	1.69	6.72	8.04	1.63

[a]A. D. Yoffe, in *Developments in Inorganic Nitrogen Chemistry*, Vol. 1, edited by C. B. Colburn (Elsevier, New York, 1966), p. 72.

as follows:

$$X(a):\ A_{2g}+A_{2u}+E_g+E_u\ ,$$

$$N(d):\ A_{1g}+A_{2g}+A_{2u}+B_{1g}+B_{1u}+B_{2g}+E_g+2E_u\ ,$$

$$N(h):\ A_{2g}+A_{2u}+E_g+E_u\ .$$

The alkali-metal anion (K, Rb, or Cs) is indicated by X and the letters in parentheses indicate the locations of the atoms in the special positions of D_{4h}^{18}. The acoustical branches have the symmetries A_{2u} and E_u. The A_{2g} vibrations are silent, that is, they do not cause a change in polarizability or dipole moment and are not optically active. The A_{2u}, B_{1u}, and E_u vibrations are infrared active. There are five possible Raman-active branches whose Raman-scattering tensors have the form[10]

$$A_{1g}:\begin{pmatrix} a & 0 & 0 \\ 0 & a & 0 \\ 0 & 0 & b \end{pmatrix};\quad B_{1g}:\begin{pmatrix} c & 0 & 0 \\ 0 & c & 0 \\ 0 & 0 & 0 \end{pmatrix};\quad B_{2g}:\begin{pmatrix} 0 & d & 0 \\ d & 0 & 0 \\ 0 & 0 & 0 \end{pmatrix};$$

$$E_g:\begin{pmatrix} 0 & 0 & e \\ 0 & 0 & 0 \\ e & 0 & 0 \end{pmatrix}\ \text{and}\ \begin{pmatrix} 0 & 0 & 0 \\ 0 & 0 & e \\ 0 & e & 0 \end{pmatrix}\ .$$

The alkali-azide crystal consists of tightly bound azide ions N$_3^-$ which are bound loosely to the anion sublattice. In such crystals where the coupling is weak between ion groups and the rest of the lattice, it is useful to label the vibrations as either internal or external. The internal vibrations are those modes in which nitrogen atoms of a given N$_3^-$ ion move with respect to one another, and the external vibrations are those modes in which the N$_3^-$ ions move as rigid units. It can be expected for XN$_3$ crystals that the internal mode frequencies will be fairly independent of the mass of the alkali-metal ion, but that the external mode frequencies should be more sensitive to anion mass.

The Raman-active phonons may be further described in terms of these external and internal motions. The A_{1g} and B_{2g} phonons are associated with the in-phase and out-of-phase symmetric stretching of the two N$_3^-$ ions in the primitive cell. This represents the crystal field splitting of the Σ_g^+ vibra-

tion associated with a free N$_3^-$ ion ($D_{\infty h}$). The B_{1g} phonon is associated with a hindered rotation of the azide ion about the z axis, the two azide ions in the primitive cell being out of phase with respect to one another. One E_g phonon is associated with the hindered rocking of the azide ion in the z direction, that is, a motion of one N(h) atom in the positive z direction and the other N(h) atom in the negative z direction, the N(d) atom remaining fixed. The remaining E_g phonon is associated with a translation of the alkali-metal ions in the plane perpendicular to the z axis, with the alkali-metal ions in adjacent planes moving in opposite directions. It should be noted that the verbal descriptions of the Raman-active phonons are intended only to be conceptually helpful.

EXPERIMENTAL

A He-Ne laser (632.8 nm, 50 mW) was used as a source of excitation. The laser radiation was focused into the crystal by an 85-mm focal length lens. The radiation scattered at right angles to the incident radiation was collected by a variable $f/1.5$ to $f/7.2$ lens system and analyzed by a SPEX model 1401 monochrometer and a photon-counting detection system. All data reported were taken with 2 cm^{-1} or less spectral slit widths, and all frequencies reported are reliable to ± 1 cm^{-1}.

Small clear crystals of potassium and rubidium azide were grown by the slow evaporation of aqueous solutions over a six-month period. The crystals possessed a truncated tetragonal pyramidal shape with well-developed (001) faces as shown in Fig. 2. The best crystals measured 2-3 mm on a side and up to 1 mm in thickness. The KN$_3$ crystals were of considerably better quality than the RbN$_3$ crystals.

It did not prove possible to grow suitable crystals of CsN$_3$. The data reported on CsN$_3$ were obtained from a thin layer of powdered sample which was pressed onto a copper block in contact with liquid
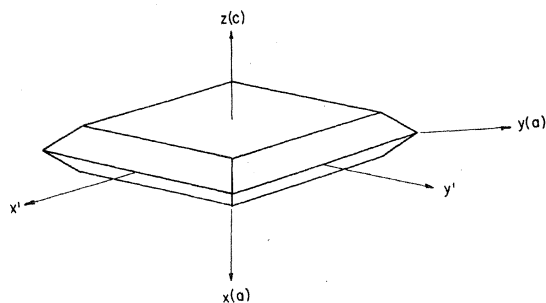
FIG. 2. Morphology of the KN$_3$ and RbN$_3$ crystals as grown by evaporation of an aqueous solution. Axes denoted $x(a)$, $y(a)$, and $z(c)$ are the crystallographic axes. Axes denoted x' and y' are a set of axes rotated 45° about the z axis from the crystallographic axes.
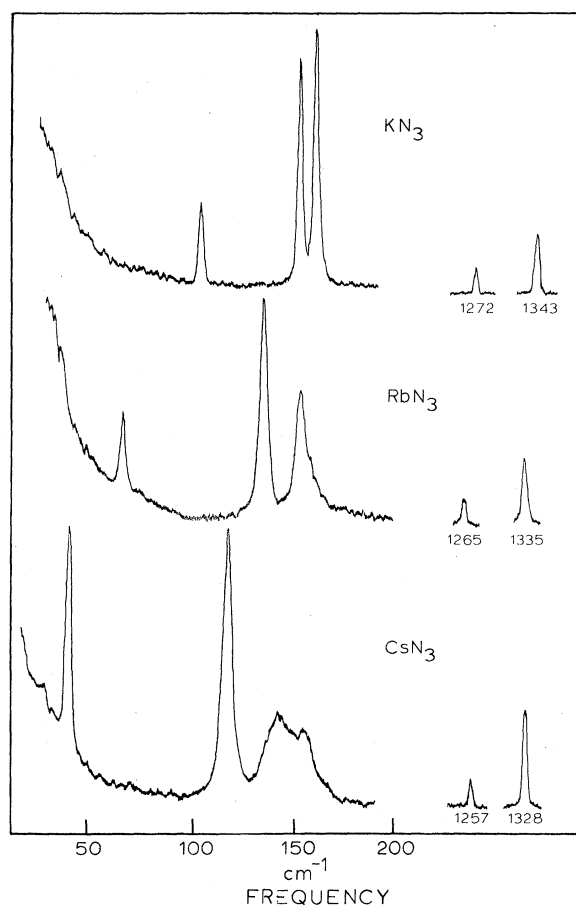
FIG. 3. Raman spectra of KN_3, RbN_3, and CsN_3 powdered samples at 82 °K; instrumental slit width of 2 cm^{-1}. All three spectra were recorded under identical experimental conditions.

The Stokes-Raman spectra for a KN_3 single crystal at room temperature for the five 90°-scattering configurations needed to uniquely define the scattering tensors are shown in Fig. 4. These data were obtained with a spectral slit width of 2 cm^{-1} and an $f/7.2$ lens. A higher-resolution (0.5 cm^{-1}) spectrum of the internal azide-ion phonons (A_{1g}, B_{2g}) for KN_3 taken at room temperature for the $y(xx)z$ and $y(xy)z$ configurations is shown in Fig. 5. These data were obtained by recording the electron pulse counts at 0.5-cm^{-1} spectral intervals for a fixed time interval. These data represent optimum alignment of the KN_3 crystal and demonstrate the best polarization separation that was obtained on the (A_{1g}, B_{2g}) internal vibrations.

nitrogen. For purposes of comparison, the powder spectra of KN_3 and RbN_3 as well as CsN_3 taken under identical conditions are shown in Fig. 3.

The crystal axes for KN_3 and RbN_3 were determined by Laue back-reflection studies and are indicated in Fig. 2. The axes indicated by $a(x)$, $b(y)$, and $c(z)$ correspond to both the crystallographic unit-cell axes and the Nye axes[11] for the Raman-scattering tensors. The axes indicated by (x') and (y') are rotated 45° about the $c(z)$ axis from the unit-cell axes.

Small crystal size and birefringence demanding critical orientation allowed the best polarization data to be obtained only with the crystal mounted on a goniometer at room temperature (298 °K). For low-temperature measurements, the KN_3 and RbN_3 crystals were mounted with thermal conducting grease on a copper block in contact with liquid nitrogen. The temperature of the sample under these conditions was measured by a thermocouple to be 82 °K.

FIG. 4. Raman spectrum of KN_3 at 298 °K; instrumental slit width of 2.0 cm^{-1}.
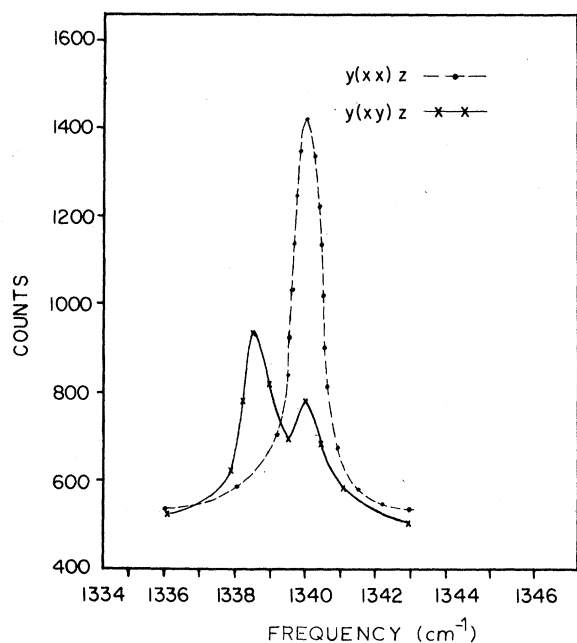
FIG. 5. Raman spectrum of the (A_{1g}, B_{2g})-ν_3 doublet for KN_3 at 298 °K; instrumental slit width of 0.5 cm^{-1}.

The observed scattering tensors for KN_3 are shown in Table II. The area of each phonon peak was measured. These values were then corrected for instrument response and these corrected values were finally normalized to the largest element $[(\alpha_{xx}^2)$ of the 152-cm^{-1} band]. These tensor values shown in Table II are reproducible to within 5%. These tensors indicate both the symmetry of the phonons and their relative scattering strengths.

Figure 6 shows the Stokes-Raman spectra for a single crystal of RbN_3 measured at 82 °K for four of the 90°-scattering configurations associated

with the x', y', z axes. It was not possible to measure scattering-tensor component values as done above for KN_3 because of poorer RbN_3 crystal quality. These data were obtained with a spectral slit width of 2 cm^{-1} and an optical aperture of $f/1.5$.

Figures 3–6 are composed of traces from the original recorder data. No corrections have been made for the changes in the instrument response with frequency. The measured frequencies for the fundamental phonons at both 298 and 82 °K for KN_3, RbN_3, and CsN_3 are presented in Table II.

DISCUSSION

All five of the Raman-active phonons of this series of alklai azides are observed in Figs. 3–6. The polarization characteristics of these Raman data for KN_3 and RbN_3 allow these phonons to be labeled according to their symmetry species. The fundamental modes of CsN_3 have been labeled by comparison with the KN_3 and RbN_3 data. These assignments are given in Table II.

As described previously, the vibrational modes of these alkali azides can be viewed as either external or internal vibrations. The external vibrations will consist of one phonon of symmetry E_g associated with a translational motion $[T(E_g)]$ of the anion sublattice, one phonon of symmetry E_g of a rotational nature $[R(E_g)]$ involving a hindered rocking of the azide ions, and one phonon of symmetry B_{1g} involving a hindered rotation of the azide ions about the z axis $[R(B_{1g})]$. Both the rotational motions associated with the N_3^- should be independent of the anion mass. The $T(E_g)$ phonon, however, should shift with increasing anion mass according to the ratio $1 : 0.68 : 0.54$ for the potassium, rubidium, and cesium ions, respectively.

The $T(E_g)$ phonon was observed to decrease in frequency from 107 cm^{-1} for KN_3 to 69 cm^{-1} for

TABLE II. Raman-active fundamental modes in K, Rb, and CsN_3.

Vibrational mode and symmetry D_{4h}	Observed frequencies (cm^{-1})						Experimentally observed Raman scattering tensors for KN_3
	KN_3		RbN_3		CsN_3		
	298 °K	82 °K	298 °K	82 °K	298 °K	82 °K	
$\nu_1(A_{1g})$	1340	1344		1336			$\begin{pmatrix} 6 & 2 & 0 \\ 2 & 6 & 0 \\ 0 & 0 & 1 \end{pmatrix}$
			1333		1327	1328	
$\nu_1(B_{2g})$	1339	1342		1335			
$R(B_{1g})$	151	165	140	158	150(±10)	145	$\begin{pmatrix} 100 & 2 & 0 \\ 2 & 100 & 0 \\ 0 & 0 & 0 \end{pmatrix}$
$R(E_g)$	145	157	128	139	121	110	$\begin{pmatrix} 0 & 2 & 54 \\ 2 & 0 & 54 \\ 54 & 54 & 0 \end{pmatrix}$
$T(E_g)$	103	107	66	69	44	46	$\begin{pmatrix} 0 & 1 & 17 \\ 1 & 0 & 17 \\ 17 & 17 & 0 \end{pmatrix}$

RbN_3 to 45 cm^{-1} for CsN_3 as the mass of the anion increases. These shifts in frequency are slightly larger than might be expected (1 : 0.64 : 0.42). The E_g character of this phonon may be seen in Figs. 4 and 6. The relative scattering intensity associated with this $T(E_g)$ phonon increased as the anion increased in size. This can best be seen in Fig. 3. Bryant[3] observed a very weak band at 65 cm^{-1} in a mercury-arc Raman spectrum of KN_3 and has labeled this band as being the $T(E_g)$ phonon. This weak band was probably caused by an impurity in the sample, perhaps RbN_3. Bryant[4] also observed a band at 42 cm^{-1} in a mercury-arc Raman spectrum of CsN_3 and has labeled this band as being E_g translational phonon in agreement with the present work. The only observation of the Raman-active vibrations of RbN_3 may be inferred from the recently reported second-order infrared transmission spectrum.[5] These data indicate a possible E_g phonon at 45 cm^{-1}. The calculations of Govindrajan and Haridasan[5] based on a rigid-ion model yield values of 74 cm^{-1} for KN_3, 49 cm^{-1} for RbN_3, and 47 cm^{-1} for CsN_3 for this E_g phonon and are at best in qualitative agreement with the present observations.

The $R(E_g)$ phonon frequency is observed to de-crease from 156 cm^{-1} for KN_3 to 139 cm^{-1} for RbN_3 to 121 cm^{-1} for CsN_3. This phonon should not shift in frequency with a change in the mass of the alkali-metal ion. The shift in frequency for the $R(E_g)$ phonon and slight departure from the expected $T(E_g)$ phonon frequency shifts may be indicative of some coupling between these two like symmetry motions. The E_g character of this phonon is seen in Figs. 4 and 6. The decrease in frequency with increase in anion size was not as marked with this phonon as with the $T(E_g)$ phonon. Furthermore, there was only a slight but not marked increase in the relative scattering intensity associated with the increase in anion size. Bryant[3] observed a band at 102 cm^{-1} for KN_3 but interpreted it to be the B_{1g} rotational phonon. The band observed at 108 cm^{-1} in CsN_3 was correctly interpreted to be the E_g rotational phonon.[4] No such phonon has been indicated by the second-order infrared transmission data for KN_3 or RbN_3.[6] Furthermore no calculated values are reported for this phonon.

The highest-frequency external vibration is the B_{1g} phonon in which the azide ions are librating out of phase about the z axis while the anion sublattice is essentially at rest. The B_{1g} character of this phonon is seen in Figs. 4 and 6. This phonon was
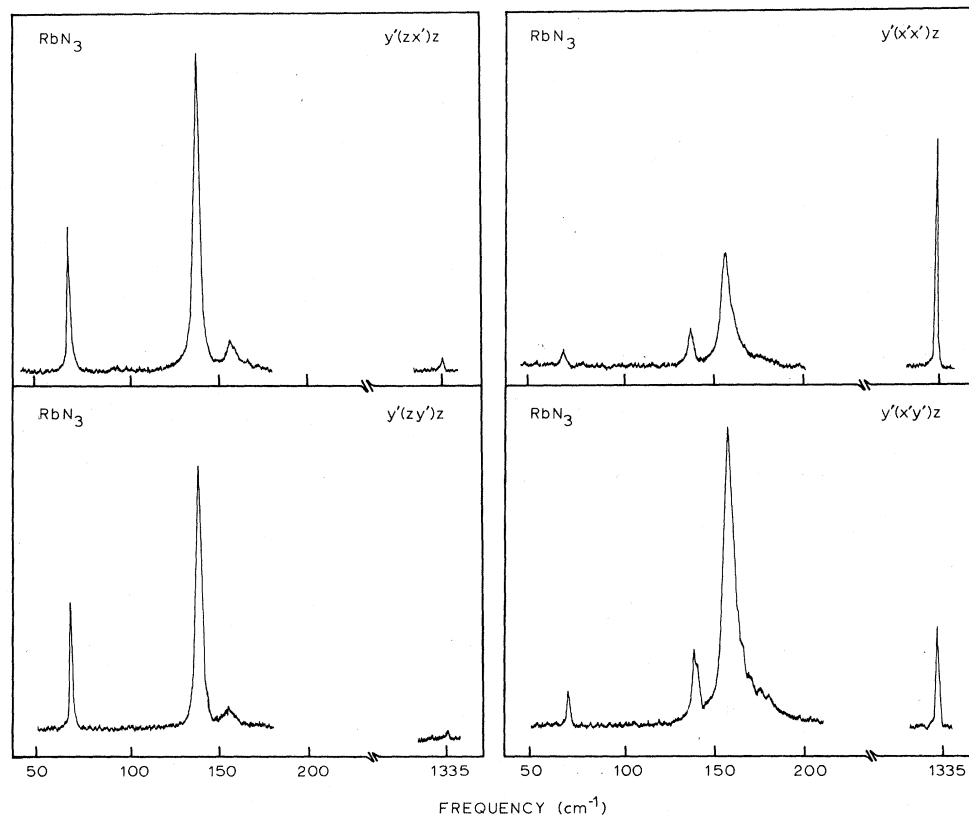
FIG 6. Raman spectrum of RbN_3 at 82 °K; instrumental slit width of 1.5 cm^{-1}. Primed axes (x', y') indicate the axes shown in Fig. 2.

observed at 165 and 158 cm^{-1} in KN_3 and RbN_3, respectively. The scattering tensor associated with a B_{1g} mode has only α_{xy} and α_{yx} components when referred to the unit-cell axes. However, if the crystal is rotated 45° about the z axis as shown in Fig. 2, the transformed B_{1g} tensor now has the diagonal form associated with the B_{2g} tensor. Similarly, the transformed B_{2g} takes the form of the B_{1g} tensor. The E_g tensors mix and the A_{1g} tensor remains unchanged under such a transformation. Data obtained from such a rotated crystal make it quite easy to distinguish between A_{1g} and B_{2g} phonons which both possess diagonal scattering tensors when referred to the unit-cell axes. Furthermore, such data also serve as a check on the B_{1g} character of any given phonon. Figure 4 shows the data obtained for a KN_3 crystal with the experimental configuration associated with the unit-cell axes. The data in Fig. 5 are for a RbN_3 crystal with the experimental configuration associated with the x' and y' axes.

The intensity and width of the B_{1g} band changed markedly as the anion size increased. This change is best seen in Fig. 3. A shoulder was observed to the high-frequency side of the 158-cm^{-1} band in RbN_3. This feature became more pronounced as a separate peak at L-N_2 temperature in the powder spectrum of CsN_3; the side-band frequencies were centered at 158 cm^{-1}. This side-band feature broadened as the temperature increased until at room temperature there was a diffuse background from approximately 140 to 200 cm^{-1}. The side-band feature was not resolved from the $R(B_{1g})$ band at room temperature. This feature has the character of a second-order process. There are numerous possibilities for second-order scattering to occur in the 150-cm^{-1} region[6] and as has been pointed out by Burstein[12] the second-order process may be enhanced in the neighborhood of a first-order phonon scattering. However, it is not clear why the width and intensity of the $R(B_{1g})$ band should change so markedly with the increase in the anion size since the contact radius remains constant.

Resolution of the E_g and B_{1g} rotational phonons would have been extremely difficult using mercury-arc excitation on polycrystalline samples. Bryant[3] has reported only a single peak for KN_3 at 147 cm^{-1} and has interpreted this to be an E_g phonon. Bryant[4] reported a broad rather weak peak centered at 153 cm^{-1} in CsN_3 and interpreted this to be a B_{1g} mode. No experimental or calculated values for the $R(B_{1g})$ phonon have been reported previously for RbN_3.

The internal vibrations of the azide ion were observed near 1330 cm^{-1} for these alkali azides. The splitting of the A_{1g}-B_{2g} doublet was 2 cm^{-1} for KN_3 at L-N_2 temperature. Figure 5 shows the A_{1g}-B_{2g} doublet for the α_{xx} and α_{xy} components at room temperature. Bryant[3] observed a strong band at 1340

cm^{-1} and a weak band at 1352 cm^{-1} and interpreted these to be B_{1g} and A_{1g} phonons, respectively. This interpretation implies the totally symmetric A_{1g} phonon is considerably less intense than the out-of-phase B_{1g} phonon and does not agree with the present polarization data. In the present study, a very weak band was observed at approximately 1352 cm^{-1} which disappeared at liquid-N_2 temperature. This temperature dependence is indicative of a multiphonon process. The normalized observed scattering tensor for the A_{1g}-B_{2g} doublet in KN_3 is given in Table II with the diagonal elements being the A_{1g} phonon and the off-diagonal the B_{2g} phonon.

A 1-cm^{-1} splitting was observed for the A_{1g}-B_{2g} doublet at liquid-N_2 temperature for RbN_3, but these phonons were not resolved at room temperature. Furthermore, no splitting was observed for these phonons in the spectrum of the powdered CsN_3. Bryant[4] observed an intense band at 1325 cm^{-1} and a weak band at 1336 cm^{-1} in CsN_3 which he interpreted to be the A_{1g} and B_{2g} vibrations, respectively. In the present study, a very weak band was observed near 1335 cm^{-1} at room temperature, but not at liquid-N_2 temperature. This temperature dependence is consistent with a multiphonon process.

While numerous weak multiphonon processes were observed in the 1250–1300-cm^{-1} spectral region at room temperature, only the $2\nu_2$ overtone was observed with any appreciable intensity at liquid-N_2 temperature. This overtone band is shown in Fig. 3.

The normalized tensors for all Raman-active fundamental phonons in KN_3 were observed to have the expected forms. The nonzero α_{xy}, α_{yx} components observed for the $R(B_{1g})$, $R(E_g)$, and $T(E_g)$ tensors may be attributed to crystal misalignment and the finite solid angles associated with the focused laser radiation and collecting optics. It is apparent from the observed tensors for KN_3 that the total scattering strengths of the $R(B_{1g})$ and $R(E_g)$ phonons are approximately equal. The scattering strength of the translational E_g phonon is considerably weaker as might be expected.

SUMMARY

The first-order Raman spectra of KN_3, RbN_3, and CsN_3 have been measured at room and liquid-N_2 temperatures. The five Raman-active phonons predicted from group theoretical considerations have been observed. The phonons have been assigned on the basis of the polarization data for KN_3 and RbN_3.

ACKNOWLEDGMENTS

†Work supported in part by the Department of Defense Themis Program through the Office of Naval Research.

[1]J. I. Bryant, J. Chem. Phys. 38, 2845 (1963).

[2]J. I. Bryant, J. Chem. Phys. 40, 3195 (1964).

[3]J. I. Bryant and R. L. Brooks III, J. Chem. Phys. 43, 880 (1965).

[4]J. I. Bryant, J. Chem. Phys. 45, 689 (1966).

[5]M. L. Malhotra, K. D. Moller, and Z. Iqbal, Phys. Letters 31A, 73 (1970).

[6]J. Govindarajan and T. M. Haridasan, Phys. Letters 28A, 701 (1969).

[7]I. R. Nair and C. E. Hathaway, Phys. Letters 30A,

253 (1970).

[8]P. A. Temple and C. E. Hathaway, Bull. Am. Phys. Soc. 15, 298 (1970).

[9]R. W. G. Wyckoff, Crystal Structures (Interscience, New York, 1964), Vol. 2.

[10]R. Loudon, Advan. Phys. 13, 423 (1964).

[11]J. F. Nye, Physical Properties of Crystals (Oxford U. P., Oxford, England, 1957).

[12]E. Burstein, in Elementary Excitations in Solids, edited by A. A. Maradudin and C. F. Nardelli (Plenum, New York, 1969), p. 367.

Structural Phase Transitions in Spinels Induced by the Jahn-Teller Effect

E. Pytte

IBM Thomas J. Watson Research Center, Yorktown Heights, New York

A dynamic theory of the cubic-to-tetragonal transformation in spinels containing octahedrally coordinated d^9 and d^4 Jahn-Teller ions is presented. Following Kanamori, the model assumes that the dominant coupling between the doubly degenerate electronic orbital and the lattice is via the elastic strain. The temperature dependence of the splitting of the degenerate electronic level and the changes in the elastic constants due to the interaction is determined. For linear Jahn-Teller coupling, the phase transition is second order. The soft mode is the acoustic shear mode propagating in the [110] direction. The frequency of this mode goes to zero at the transition temperature and remains zero in the distorted structure. Including third-order Jahn-Teller coupling, the phase transition becomes first order. The shear sound velocity changes discontinuously at the transition temperature and then increases with decreasing temperature.

I. INTRODUCTION

This paper considers structural transitions from cubic to tetragonal symmetry in spinel structures containing d^4 and d^9 transition-metal ions. The connection between these phase transitions and the Jahn-Teller effect was first recognized by Dunitz and Orgel[1] and by McClure.[2] Several thermodynamic theories were subsequently constructed. Those by Finch, Sinha, and Sinha[3] and by Wojtowicz[4] considered the case of large local distortion due to the static Jahn-Teller effect. At high temperatures, these distortions are oriented randomly among three equivalent positions. Due to interactions between the distortions, a transition occurs to an ordered structure with all the local distortions aligned in one particular direction. This occurs when the interaction energy gained by aligning the distortions becomes more effective in lowering the free energy than the entropy, which favors a random distribution of the distortions among the equivalent positions. This model corresponds to the case of strong local anisotropy in which the anisotropy energy is much larger than kT_c where T_c is the transition temperature.

The more recent work by Englman and Halperin[5]

extends the work by Wojtowicz by taking into account the dynamic Jahn-Teller coupling and the excited vibrational states. Due to the interaction between the Jahn-Teller complexes, the localized vibrational modes associated with a single complex assume the character of propagating optical phonons. However, the interaction was treated in a molecular-field theory and thus only the $q = 0$ limit was discussed. Interaction of the electronic system with acoustic phonons was not considered.

A basically different model has been considered by Kanamori.[6] This model describes the spontaneous appearance of a local distortion at the transition temperature. The model implicitly assumes that the interaction between neighboring distortions is sufficiently strong to immediately align the local distortions once these appear. In this model (in its simplest form), there is no local distortion above the transition temperature.

For the case of the normal spinels $FeCr_2O_4$ and FeV_2O_4 with Fe^{2+} Jahn-Teller ions at tetrahedral sites, Mössbauer experiments show that considerable local distortion persists above the transition temperature.[7] However, for Jahn-Teller ions at octahedral sites the amount of local distortion cannot be measured by the Mössbauer effect because